Anisotropy and memory during cage breaking events close to a wall

Matthias Kohl[1], Andreas Härtel[2],* and Michael Schmiedeberg[3†]
[1] *Institute for Theoretical Physics II: Soft Matter, Heinrich Heine University Düsseldorf, Universitätsstr. 1, D-40225 Düsseldorf, Germany*
[2] *Institute of Physics, Johannes Gutenberg-University Mainz, Staudinger Weg 9, 55128 D-Mainz, Germany*
[3] *Institute for Theoretical Physics I, Friedrich-Alexander-University Erlangen-Nürnberg, Staudtstr. 7, D-91058 Erlangen, Germany*

The slow dynamics in a glassy hard-sphere system is dominated by cage breaking events, i.e., rearrangements where a particle escapes from the cage formed by its neighboring particles. We study such events for an overdamped colloidal system by the means of Brownian dynamics simulations. While it is difficult to relate cage breaking events to structural mean field results in bulk, we show that the microscopic dynamics of particles close to a wall can be related to the anisotropic two-particle density. In particular, we study cage-breaking trajectories, mean forces on a tracked particle, and the impact of the history of trajectories. Based on our simulation results, we further construct two different one-particle random-walk models – one without and one with memory incorporated – and find the local anisotropy and the history-dependence of particles as crucial ingredients to describe the escape from a cage. Finally, our detailed study of a rearrangement event close to a wall not only reveals the memory effect of cages, but leads to a deeper insight into the fundamental mechanisms of glassy dynamics.

arXiv:1610.07846v1 [cond-mat.soft] 25 Oct 2016

This is the Accepted Manuscript version of an article accepted for publication in Journal of Physics: Condensed Matter. IOP Publishing Ltd is not responsible for any errors or omissions in this version of the manuscript or any version derived from it. The Version of Record is available online at http://dx.doi.org/10.1088/0953-8984/28/50/505001.

I. INTRODUCTION

Hard spheres with solely steric repulsion are an important model system in the field of soft condensed matter as they exhibit not only a fluid and a crystalline phase [1], but there occurs a dramatic slowdown of dynamics when also the density of the particles is increased [2, 3]. The relation of this slow dynamics within a glassy system to structural properties is an important topic of ongoing (theoretical) research [4–12] and aims on a deeper understanding of the major mechanisms that dominate glassy dynamics.

Many theoretical approaches to describe glassy dynamics are based on cage breaking events, e.g., the widely-used mode coupling theory [5, 14] or models that consider activated hopping of particles out of a cage [7, 8, 11, 12]. Such mean-field theories are usually based on an isotropic average cage around the considered particle such that effects arising from the anisotropic structure of a cage are ignored. To avoid this drawback, we consider a cage close to a flat wall such that isotropy is broken. An example of a particle that is trapped by a cage of neighboring particles close to a wall is sketched in Fig. 1(a). Since isotropy is broken, we have the advantage to know the preferred escape route from the cage (indicated by an arrow in Fig. 1(a)). Our goal is to identify the essential ingredients that are necessary to develop an one-particle random-walk model that is able to describe the escape dynamics. Furthermore, our analyzes of the anisotropic cage-breaking event also opens another view on cage-breaking events in bulk, where cages are only isotropic in a mean field description due to averaging over different directions. Such an averaging might lead to mistakes when the dynamics along escape routes should be predicted.

By using (classical) density functional theory (DFT), the anisotropic two-particle correlation functions and, therefore, the structure of a cage that traps a particle close to a wall can be determined theoretically [13, 15] (the full gamut of classical DFT is covered in [16]). As we will show later, structural results will be important to understand the anisotropic cage breaking dynamics. For the system that we consider here, we have resolved the anisotropic structures in a previous work [13], where we studied a glass-forming binary hard-sphere mixture close to a wall by applying the White Bear mark II framework of fundamental measure theory [17], a quantitative benchmark DFT for hard spheres [18, 19]. We found very good agreement between DFT and Brownian dynamics (BD) computer simulations and could observe cage-forming structure. A typical result is shown in Fig. 1(b), where the total correlation function (the pair distribution function follows by adding a constant) is shown for a small particle in contact with the wall. Both the correlations with neighbouring small (upper panel) and large (lower panel) particles have preferred positions for finding a neighbouring particle. This anisotropic structure can not be found from solely one-particle correlations, which are often studied in order to understand surface free energies and the adsorption of particles to walls [18, 20, 21].

* AnHaerte@uni-mainz.de
† michael.schmiedeberg@fau.de

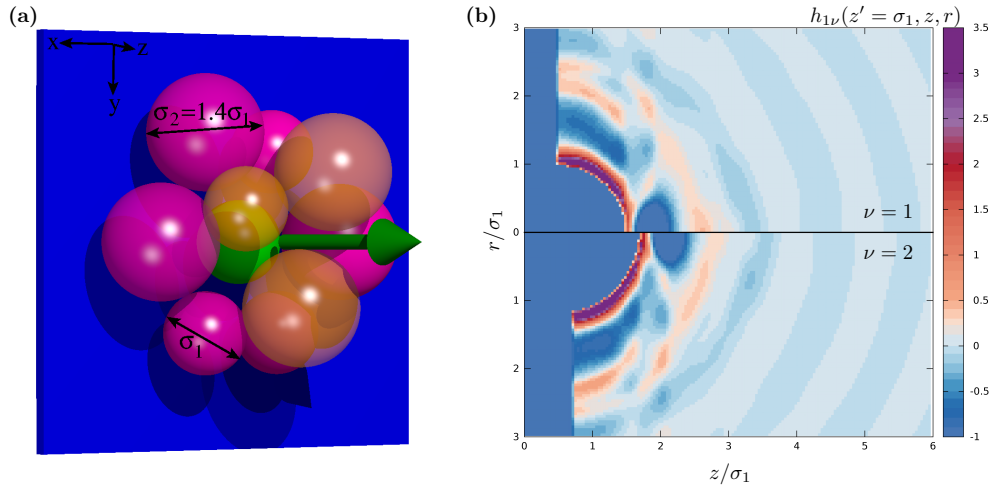

Figure 1. (a) Schematic sketch of a particle (shown in green) with diameter σ_1 close to a wall. The particle is trapped in a cage formed by its neighbors with diameters σ_1 or $\sigma_2 = 1.4\sigma_1$. The z axis is aligned perpendicular to the wall plane, which is located at $z = 0$. Note that the coordinate system in the figure only denotes the directions of the axis. The origin is located at the wall at the projected position of the trapped particle, i.e., the latter is located at the radial coordinate $r = \sqrt{x^2 + y^2} = 0$. (b) Two-particle pair correlation function as studied in previous work [13] by DFT and BD simulations. Here, we show data from DFT for a total packing fraction $\phi = 0.56$, where a small particle is located at the wall and its neighbors form a cage. The upper panel shows the correlations between the trapped particle and the other small particles, the lower panel those between the trapped particle and the large particles. More details and further examples on the structure of such a system can be found in [13].

In Sec. II we introduce our model system and explain details of the Brownian dynamics simulations. The dynamical self-correlation functions of a cage-braking event are determined and discussed in Sec. III. In Sec. IV, we explore the properties of a cage, namely the force that acts on a caged particle due to its anisiotropically distributed neighbours, the collision frequency when the trapped particle inside tries to escape, and the history-dependence of the cage-breaking event. These properties are used as ingredients to develop one-particle random-walk models as explained in Sec. V. Finally, we conclude in Sec. VI.

II. MODEL SYSTEM

In this work we study a binary mixture of purely repulsive soft spheres in a solvent and in the vicinity of a wall by means of BD simulations, i.e., the solvent is captured by considering random kicks and in contrast to Newtonian dynamics no inertia effects occur. Half of the particles possess the effective diameter σ_1 and the other half has a larger diameter $\sigma_2 = 1.4\sigma_1$. Usually we consider 32000 particles in a three dimensional cubic box with periodic boundary conditions in two directions (the x- and y-direction in our choice of the coordinate system) and closed by two walls normal to third direction (the z-direction). We typically combine the number densities $\bar{\rho}_\nu$ of each species ν in a total packing fraction $\phi = \sum_\nu \frac{\pi}{6}\sigma_\nu^3\bar{\rho}_\nu$. The spheres, as sketched in Fig. 1(a), interact according to the potential

$$u_{\nu\nu'}(\Delta) = \begin{cases} \frac{\varepsilon}{2}\left(1 - \frac{\Delta}{\sigma_{\nu\nu'}}\right)^2 & \Delta \leq \sigma_{\nu\nu'} \\ 0 & \text{otherwise,} \end{cases} \tag{1}$$

where Δ is the separation of two interacting spheres, $\sigma_{\nu\nu'} = (\sigma_\nu + \sigma_{\nu'})/2$ involves the effective particle diameters σ_ν, and ε denotes the strength of the interaction. The particle-wall interaction is given by a similar harmonic potential with the same strength factor ε. In the limit of small temperatures T and large interaction strengths, i.e. for $\varepsilon/k_\mathrm{B}T \gg 1$ with Boltzmann's constant k_B, the structure and dynamics of the system correspond to the structure and dynamics of a hard sphere system [13, 22–28]. We have chosen ε such that for a given temperature the average overlap between two particles or between a particle and the wall does not exceed 5% of the diameter σ_1 (see also [13]).

The dynamics of our BD simulations is given by the overdamped Langevin equation

$$\gamma_\nu \dot{\vec{r}}_{\nu,i}(t) = \vec{f}_{\nu,i}\left(\left\{\vec{r}_{\nu',1}, \ldots, \vec{r}_{\nu',N_{\nu'}}\right\}_{\nu'=1,2,\ldots}\right) + \vec{\xi}_{\nu,i}(t)\,. \tag{2}$$

The friction constants γ_ν are proportional to the diameter σ_ν of the spheres. The pair interaction forces between the particles and between the particles and the walls are taken into account in $\vec{f}_{\nu,i}$. The thermal kicks due to a given temperature T are included by random forces $\vec{\xi}_{\nu,i}(t)$ that are chosen from a Gaussian distribution with zero mean value and second moments given by

$\left\langle \vec{\xi}_{\nu,i}(t)\vec{\xi}^{\mathrm{T}}_{\nu',i'}(t')\right\rangle = 2\gamma_\nu k_\mathrm{B}T\delta_{\nu\nu'}\delta_{ii'}\delta(t-t')\mathbb{1}$, where $\vec{\xi}^{\mathrm{T}}_{\nu'}$ is the transpose of $\vec{\xi}_{\nu'}$ and $\mathbb{1}$ is the three-dimensional unit matrix. We employ $\tau_B = \sigma_1^2/(3\pi D_1)$ as a suitable Brownian time throughout the article, where D_1 is the coefficient of free diffusion of the small spheres. More details about the simulations and an analysis of the hard sphere limit are given in a previous work [13], where we studied the structure of a binary hard-sphere system in the vicinity of a hard wall by simulations and DFT calculations.

III. DYNAMICAL CORRELATIONS OF ANISOTROPIC CAGE-BREAKING EVENTS

In dense systems each particle is surrounded by a cage of neighboring particles (see for instance Fig. 1). In bulk such a cage can possess any orientation and, for this reason, a mean field description usually is isotropic. Instead, close to walls a preferred orientation of the cage exists. It occurs more often than other configurations. Consequently, preferred escape routes exist for cage-breaking events, too. In this section we study dynamical time-dependent van Hove self-correlation functions obtained from simulations in order to explore the anisotropy of cages and to identify preferred escape routes.

In Fig. 2, we plot simulation results of the van Hove self-correlation function $G_\nu(r,z;t)$ [29]. The function represents the probability density for a particle of species ν to be at the position (r,z) after a time t, if it was tracked in the origin $(0,0)$ at time 0. Due to the symmetry of the system under investigation, we represent the position of a particle in cylindrical coordinates (r,z), i.e. the distance z from the wall and the distance r from the z-axis (cf. Fig. 1). The van Hove function represents the information about the diffusion pathways or preferred particle trajectories. Figure 2(a) displays $G_1(r,z;t)$ for small particles (first row) and $G_2(r,z;t)$ for large particles (second row) at a volume fraction $\phi = 0.50$ and for different evolution times, as indicated. The caging of particles is visible in the slowed down diffusive dynamics for shorter times (Fig. 2, (a1-a3) and (a6-a8)). Of course, diffusion is prohibited inside the wall, but the overall diffusion process in all remaining directions still looks rather homogeneous as long as the particle does not leave its cage. For a density close to the glass transition (see Fig. 2(b) for $\phi = 0.58$), $G_\nu(r,z;t)$ displays an even slower diffusion process (note the different timescales). On the same time, the diffusion within the cage becomes more anisotropic, e.g., while in Fig. 2(a2) no preferred direction of motion is visible, close to the glass transition as shown in Fig. 2(b2) a particle within a cage more likely moves parallel to the wall and the motion in all other directions is suppressed. In all cases, the small particles diffuse faster as expected from the smaller friction constant γ_1.

For sufficiently long times, we can identify different escape routes along which the particle can leave the cage. Besides a diffusive spread within the first layer in direction parallel to the wall, smaller particles tend to use a perpendicular path to swap into the second layer (Fig. 2, (b2-b3)) before they spread in parallel directions again (Fig. 2, (b4-b5)). For the large particles, however, the typical diffusion paths are different. First, when large particles approach the second layer, they spread much slower along the second layer (Fig. 2, (b6-b8)) than the small particles do. Second, when large particles arrive at a distance of approximately $1.7\sigma_1$, their most likely trajectories branch away from the z-axis, while small particles also stay at the z-axis (Fig. 2, (b9-b10) and (b4-b5)). This can be explained by a preferred stacking of large particles above small particles. If a large particle was initially located next to a small one, it raises towards the second layer until it is possible to stack with its smaller neighbor. In order to do so, it leaves the actual perpendicular path. The last plot of the time series of the large particles' van Hove function (Fig. 2, (a10 and b10)) suggests that first isolated peaks evolve before the probability density washes out in the second layer. These two mechanisms, namely the perpendicular diffusion of the small and the tilted diffusion of the large particles, account for local rearrangement processes. Such rearrangements also occur in the bulk case, but due to isotropy with no preferred direction. Due to our symmetry breaking wall, in our situation the probability densities $G_\nu(r,z;t)$ are anisotropic and bear pre-defined more probable diffusion paths due to the structure of the local neighborhood.

To quantify this effect we explore the consequences of the anisotropic escape routes for the directional dependence of the mean squared displacements (MSD). As we will show in the following, the diffusion process and the accompanied escape from the cage into a certain direction are similar to the diffusion and escape in all other spatial directions, but each event must be weighted with the probability for its occurrence. In Fig. 3 we plot the normalized MSDs obtained from our BD simulations for small particles in different directions, i.e. in z-direction:

$$\left\langle \Delta z(t)^2\right\rangle = \frac{1}{N_1}\sum_{i=1}^{N_1}\big(z_i(t)-z_i(0)\big)^2, \tag{3}$$

in direction parallel to the wall (radial in the cylindrical coordinates):

$$\left\langle \Delta r(t)^2\right\rangle = \left\langle \Delta x(t)^2\right\rangle + \left\langle \Delta y(t)^2\right\rangle, \tag{4}$$

and in radial (spherical coordinates) direction in a certain solid angle range $[\vartheta_\mathrm{I},\vartheta_\mathrm{II}]$:

$$\begin{aligned}&\left\langle \Delta\vec{r}(t)^2\right\rangle_{[\vartheta_\mathrm{I},\vartheta_\mathrm{II}]}\\ &= \frac{1}{N_1'}\sum_{i=1}^{N_1}\theta\big(\vartheta_i(t)-\vartheta_\mathrm{I}\big)\theta\big(\vartheta_\mathrm{II}-\vartheta_i(t)\big)\big(\vec{r}_i(t)-\vec{r}_i(0)\big)^2.\end{aligned} \tag{5}$$

Here, we applied the Heaviside step function $\theta(\cdot)$ and the number of considered particles N_1', i.e., the number of non-zero addends, for particles that fulfill the criterion. Note that for simplicity we have omitted the index

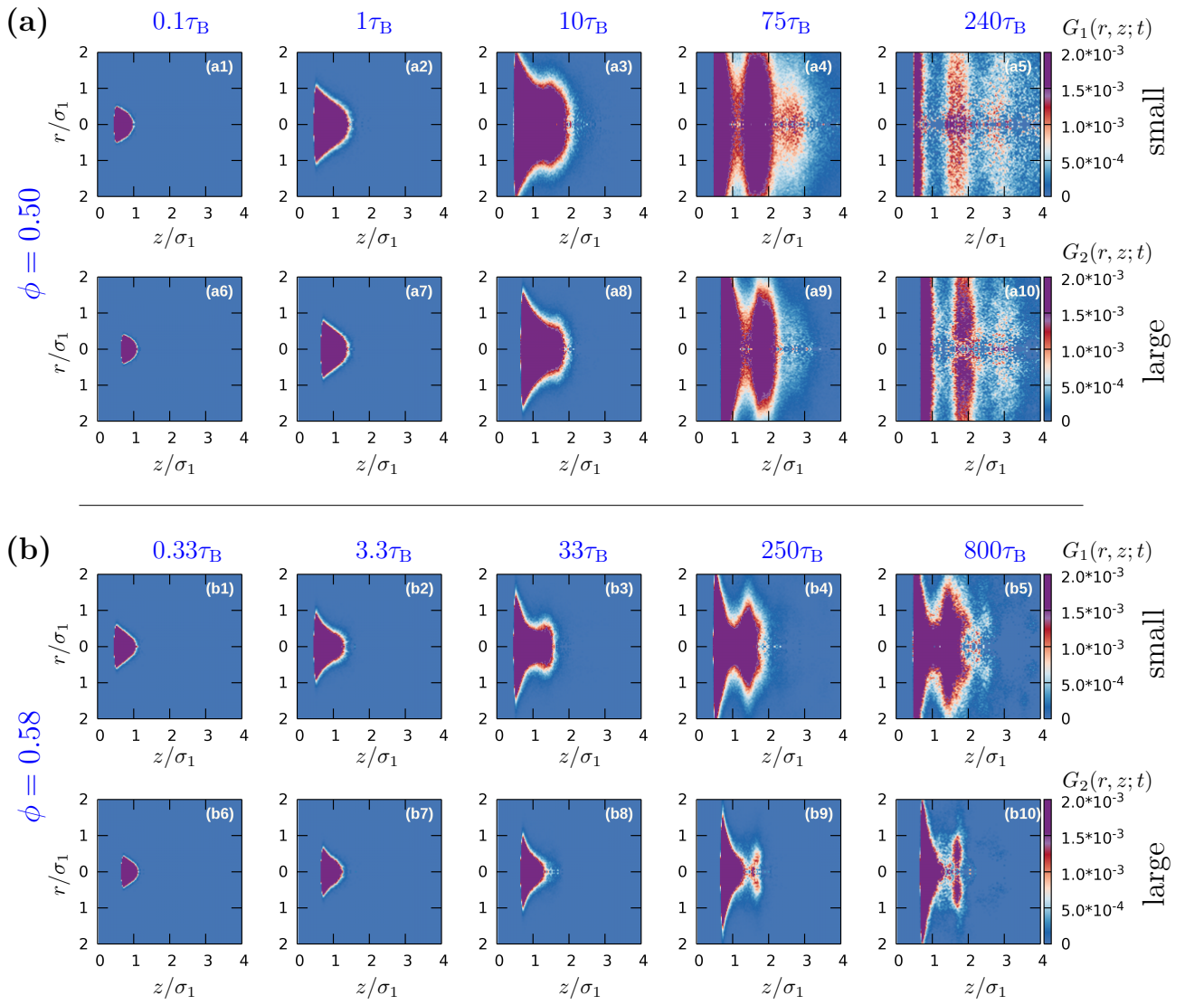

Figure 2. Self parts of the van Hove correlation function $G_\nu(r,z;t)$ for (a) $\phi = 0.50$ and (b) $\phi = 0.58$. The cylindrical coordinates z and r represent the distance from the (left) wall located at $z = 0$ and the distance from the z-axis, at which the traced particle is located initially at $t = 0$. Plots from the left to the right show the functions $G_\nu(r,z;t)$ after different time (in units of the Brownian time τ_B), as indicated at the top of each column in panels (a) and (b). The upper row of each panel (a1-a5 and b1-b5) represents data for small particles ($\nu = 1$), whereas the lower row of each panel (a6-a10 and b6-b10) represents data for the large particles ($\nu = 2$). Note that the timespan in (a) is smaller than in (b). The color code is the same for all plots and given on the right side of each line.

$\nu = 1$ for small particles. Equation (5) represents the diffusion process of selected particles that move only into the desired direction. Their final positions after a time t, denoted by the polar angles $\vartheta_i(t)$, are restricted to $\vartheta_I \leq \vartheta_i(t) \leq \vartheta_{II}$.

The MSDs from Fig. 3(a) are calculated with respect to different starting positions, i.e., $z(t = 0)/\sigma_1 = 0.55, 0.95, 1.55$, where in Fig. 3(b-d) the particles always start at wall contact. As it is clearly visible in Fig. 3(a), the effect of different starting positions has major impact on the shape of the vertical short-time MSD at intermediate or high packing fractions. If the tracked particle starts inside a layer, i.e., the maximum of the density profile (at $z_1/\sigma_1 = 0.55, 1.55$), it immediately feels the impact of the confining cage at this position. This fact makes it to become trapped at short and intermediate times and only jump after larger waiting times. Furthermore, if a particle starts in the second layer, it is able to jump forward or backward. Therefore, especially at shorter times the diffusion is enhanced by a factor of approximately 2 with respect to a particle that starts in front of the wall. However, the initial trapping in the cage is still visible. At larger times, backward jumps are restricted by the wall and the factor 2 disappears. Contrarily, if the starting position is in between the first two layers ($z_1/\sigma_1 = 0.95$), the diffusion in z-direction is

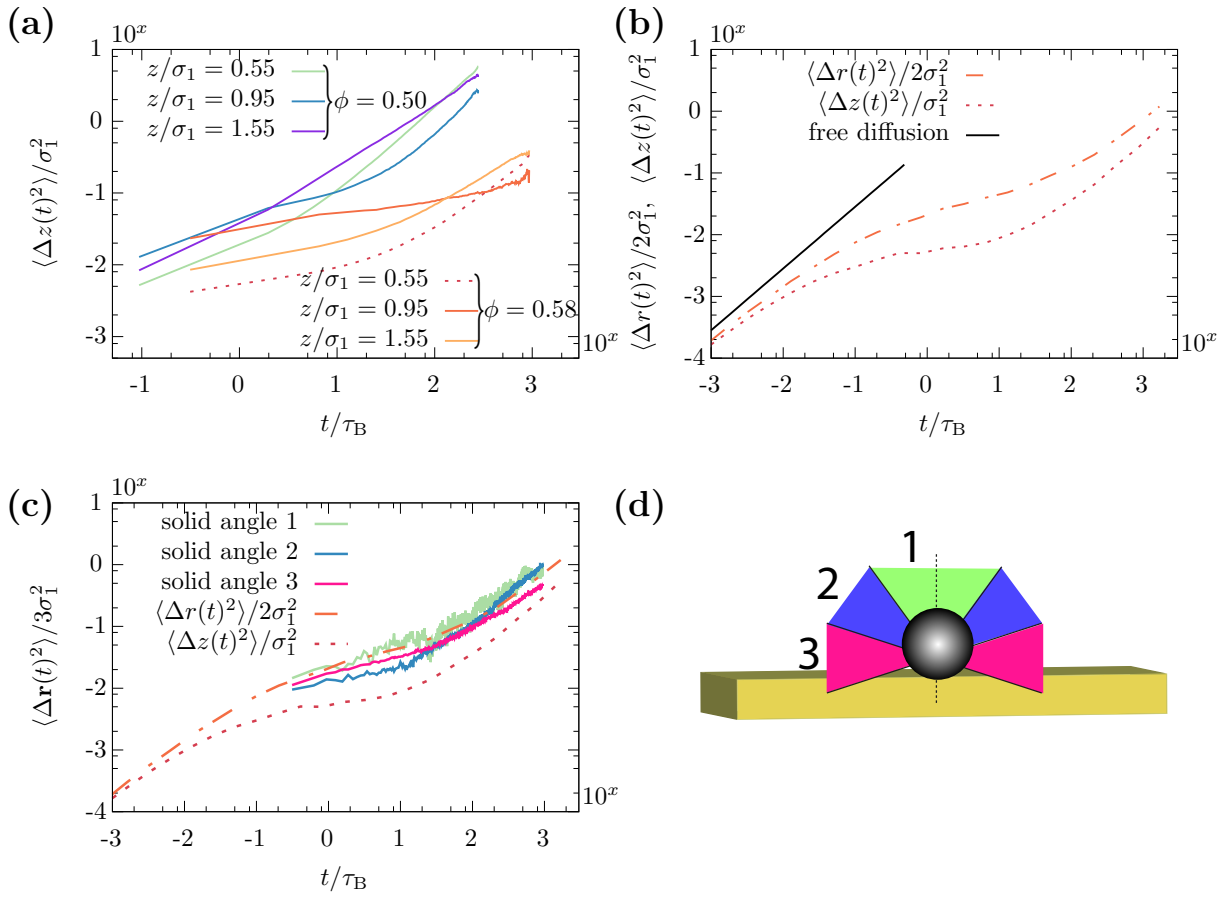

Figure 3. Double logarithmic plots of the mean squared displacements (MSD) of small particles (species $\nu = 1$) in a binary mixture. (a) The MSDs in z-direction for two packing fractions and three different starting positions of the respective trajectories. (b) MSD parallel ($\langle \Delta r^2 \rangle$) and perpendicular ($\langle \Delta z^2 \rangle$) to the wall for a packing fraction $\phi = 0.58$. For comparison, the theoretical curve of free diffusion is shown by a solid black line. (c) The dashed curves are the same as in (b), whereas the solid lines represent normalized radial MSD ($\langle \Delta \tilde{r}^2 \rangle_{[\vartheta_I, \vartheta_{II}]}$), for which the averages have only been performed over a subset of particles that have moved into given directions within the solid angle ranges as sketched in (d) and labeled with (1,2,3). The intervals in the standard representation of the polar angle ϑ are (1)=$[0, \pi/5]$, (2)=$[\pi/5, 2\pi/5]$, and (3)=$[2\pi/5, 3\pi/5]$.

larger for short times and smaller for long times. This is due to the fact that the starting position for such a particle is less stable, because it is unfavorable to stay in between two layers. Successively, when the particle relocates along the z-axis, it inevitably reaches one of the neighboring layers, where it might be caught in a cage for a typical period. Since we aim to investigate the local rearrangement from one stable position to another, we will always consider particles that start at the wall in the following.

In Fig. 3(b) we plot the MSD (averaged over all small particles) for a dense system with packing fraction $\phi = 0.58$ for directions parallel and perpendicular to the wall in comparison with the free diffusion. The averaged curves suggest that the diffusion process in z-direction is stronger suppressed than parallel to the wall. This is because we consider the average over all particles in Fig. 3(b). However, if only particles within the preselected directions are employed, the different MSD look all rather akin as demonstrated in Fig. 3(c). All curves approximately correspond to the curve of the diffusion along the wall from Fig. 3(b). This intriguing finding leads to the conclusion that the diffusion behaves similar in all spatial directions, where at the same time diffusion along the wall is more probable (already seen from Fig. 2). Only because in the usual representation of the MSD the displacement is weighted by the probability of the accompanied sampling in a certain direction, a more pronounced plateau emerges when inspecting less probable directions, e.g., as in Fig. 3(b).

One has to be careful with the interpretation of the above presented averages, since a particle could for example escape in a tilted direction due to the lack of a neighboring particle at that position, by chance. Such events would occur in the direction where the first and second layer in Fig. 1(b) are connected by strongly correlated regions, i.e., along a path on which the minimal value of the total correlation function is as large as possible. Note that its direction is also captured by the solid angle interval 1 in Fig. 3(d).

Still, the above described perceptions motivate for the fact, that the escape in other directions can probably be treated in a similar way as the perpendicular escape, just with the difference that some directions are more probable than others. Concerning the importance for the bulk, the completely averaged diffusion process is probably the result of the weighted composition of the separate diffusion mechanisms in all possible directions.

For this reason, we will focus on the cage escape in z-direction within our setup in the following sections. In particular, we will study the forces acting on a particle during its escape, relate the forces to collision frequencies in a hard-sphere system, and investigate the history dependence of escape paths.

IV. PROPERTIES OF ANISOTROPIC CAGES AND CAGE-BREAKING EVENTS

In this section we analyze the forces acting on a sphere that is trapped in an anisotropic cage formed by its neighboring particles. Furthermore, we explore the history dependence of the dynamics during cage-breaking events. The properties studied in this section will be used as ingredients for the one-particle random-walk models proposed in Sec. V.

IV.1. Force distribution at finite temperatures

While in the previous section we focused on the preferred trajectories which trapped particles use to escape from cages, we now look for mean forces on particles during their escape. In order to explore the properties of a cage, we use the BD simulations to calculate the mean forces $\langle f_{1,\perp}(z,\vartheta)\rangle$ that act on the surface of a small particle. These forces arise from overlaps with neighboring particles which are located in directions denoted by the polar angle ϑ. Figure 4(a) shows these forces averaged over a large number of configurations in a dense system with $\phi = 0.58$ for various distances z from the wall. The two very prominent peaks in all the distributions stem from the likely configurations where the small test particle is the neighbor of a small or a large sphere at the wall, respectively. As the tracked particle detaches from the wall, these peaks shift from the sides towards the bottom hemisphere ($\vartheta = \pi$) of its surface (if the wall is considered at the bottom of the box). However, from atop ($\vartheta = 0$) the forces become smaller. This is due to the unfavored position of a neighboring particle on top of the test particle, because particles of the second layer from the wall are usually not positioned directly on top of particles of the first layer (cf. structural analysis in previous work [13]). This explains our results of the van Hove functions, where the direction perpendicular to the wall is the preferred direction for a small test particle to move.

In order to obtain the forces that a particle has to overcome in order to move in a certain direction, we average all force components acting along the opposite direction over the hemisphere of the test particle that points in the corresponding direction. To be specific, for a direction given by a vector

$$\vec{a}(\vartheta,\varphi) = \sin(\vartheta)\cos(\varphi)\vec{e}_{\mathrm{x}} + \sin(\vartheta)\sin(\varphi)\vec{e}_{\mathrm{y}} + \cos(\vartheta)\vec{e}_{\mathrm{z}} \quad (6)$$

we calculate the average

$$\langle f_{1,\circ}(z,\vartheta)\rangle = \langle f_{1,\perp}(z,\vartheta')\vec{a}(\vartheta',\varphi')\cdot\vec{a}(\vartheta,0)\rangle_{\vartheta',\varphi'}, \quad (7)$$

where $f_{1,\perp}(z,\vartheta')$ is the normal force on the surface along direction ϑ' as plotted in Fig. 4(a). The average $\langle\cdot\rangle_{\vartheta',\varphi'}$ is taken over the angles ϑ' and φ' denoting a hemisphere around the direction given by ϑ. Examples of such hemispheres are shown in Fig. 4(c) for $\vartheta = 0$ and $\vartheta = \pi/4$. We call $\langle f_{1,\circ}(z,\vartheta)\rangle$ the cross section force.

Results for the cross section forces are shown in Fig. 4(b) as functions of the direction for different particle positions z. The curves represent forces that a particle has to countervail in order to move into a certain direction. One can nicely see the change of the forces with the angle and the particle detachment. When a particle is close to contact (red line in Fig. 4(b)), the cross section force exhibits a strong minimum for the direction pointing towards the wall ($\vartheta = \pi$). Note that the particle hardly can move into that direction due to the repulsion from the wall that is not included in the particle-particle force considerations. In the opposite direction ($\vartheta = 0$) a subtle local minimum occurs and there is a maximum into a tilted direction ($\vartheta \approx \pi/4$) roughly denoting the direction towards the neighboring particles in the second layer (compare also Fig. 1(b)). As the test particle is moved away from the wall towards the middle of the first two density layers, the minimum in the direction perpendicular away from the wall ($\vartheta = 0$) becomes even more pronounced, whilst the maximum shifts towards the parallel direction (see, e.g., the cases represented by the yellow/green lines).

Note that the cross section force cannot be calculated from a one-particle density, but at least a two-body description as presented in previous work [13] is needed, because the anisotropy of the force distribution is crucial.

IV.2. Collision frequency in the hard-sphere limit

Besides the above discussed directional anisotropies, another ingredient matters for the interaction between the particles. In a perfect hard-sphere system the particles only interact upon collision and are force free most of the time. In order to determine how often such collision events occur, we analyze the distribution of the absolute value of the interaction force for our soft-sphere system where the overlapping energy is well-defined and then approach the hard-sphere limit.

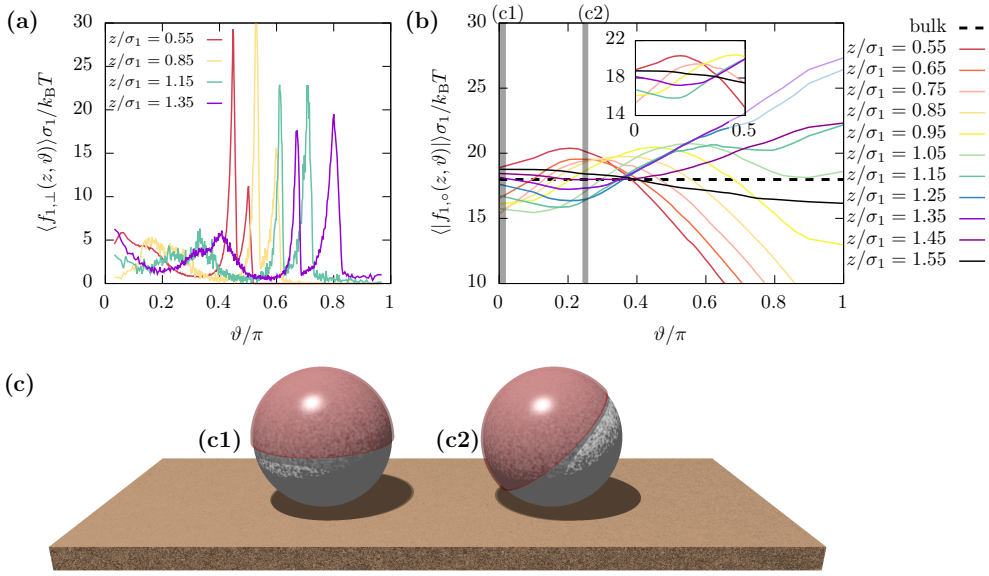

Figure 4. (a) Distribution of the mean normal forces $\langle f_{1,\perp}\rangle$ that act on a small particle from different directions in a binary mixture with overall packing fraction $\phi = 0.58$ and for various distances z from the wall. The angle ϑ denotes the direction of the force and is measured with respect to the z-axes, where $\vartheta = 0$ corresponds to forces acting towards the wall. (b) Cross section forces $\langle f_{1,\circ}\rangle$ obtained by averaging over all force contributions that act along a direction denoted by ϑ on the half sphere pointing in that direction. This corresponds to the forces that the particle has to overcome in order to move in the corresponding direction. The direction-independent bulk value is given for comparison by a dashed black line; z again denotes the distance from the wall. The inset highlights the behavior on hemispheres that point away from the wall. (c) Two examples for particles with marked hemispheres for (c1) $\vartheta = 0$ and (c2) $\vartheta = \pi/4$. The corresponding positions are highlighted by vertical gray stripes in panel (b).

The Boltzmann factor for two particles of the species ν and ν' with the interaction potential $u_{\nu\nu'}(d)$ is proportional to the probability of finding those two particles with an overlap d. It is given by

$$P_{\nu\nu'}(d) \propto \exp\left[-\frac{u_{\nu\nu'}(d)}{k_BT}\right] = \exp\left[-\frac{|f|^2\sigma_{\nu\nu'}^2}{2\varepsilon k_BT}\right], \qquad (8)$$

where $f = \frac{\epsilon}{\sigma_{\nu\nu'}}\left(1 - \frac{\Delta}{\sigma_{\nu\nu'}}\right)$ is the force according to our harmonic model potential as given in Eq. (1). Therefore, the last term in Eq. (8) is the probability how often a certain force occurs.

In Fig. 5(a) we show the force distribution obtained from simulations at different temperatures. For low temperatures the simulation results can be fitted with a Boltzmann-factor for the mixture that we employ in simulations, i.e.,

$$P(|f|) = \frac{A\sigma_1}{4\varepsilon}\sum_{\nu,\nu'=1,2}\exp\left[-\frac{|f|^2\sigma_{\nu\nu'}^2}{2\varepsilon k_BT}\right], \qquad (9)$$

where A is a dimensionless fitting parameter. For temperatures below $10^{-4}k_BT$, the fits in Fig. 5(a) become sufficiently good and the factor of the distribution stays constant. Therefore, if we calculate the first moment of the distribution, $\langle|f|\rangle \equiv \langle|f|, P(|f|)\rangle$, the result (Fig. 5(b)) is inversely proportional to the temperature, as it should be. Since the force distributions follow a Gaussian, the expectancy value of a modified normalization only over non-zero forces must be proportional to $A\sqrt{k_BT}$. The simulation results are shown in Fig. 5(c) together with a square root power-law, $P_{1,\text{coll}} \propto \sqrt{k_BT}$, which can be applied as a prediction of the fraction of interacting (or colliding) particles at low temperatures, where sufficiently below jamming particles exhibit only one or zero overlaps.

If the factor A is known, one can then deduce the collision probability

$$P_{1,\text{coll}} = \frac{A}{8}\sqrt{\frac{2\pi k_BT}{\varepsilon}}\sum_{\nu,\nu'=1,2}\frac{\sigma_1}{\sigma_{\nu\nu'}}. \qquad (10)$$

This ingredient will be used in section V to develop a random walk model for a single tracer particle in front of the wall, which interacts with its environment, just with a probability equal to $P_{1,\text{coll}}$. For our random walk models, we will determine the factor A from fits to simulation data as shown in Fig. 5(a). Note that in principle A for the hard sphere limit also could be estimated by calculating the average force expected from the bulk equation of state of hard spheres, i.e., obtained from DFT with the White Bear mark II functional [17].

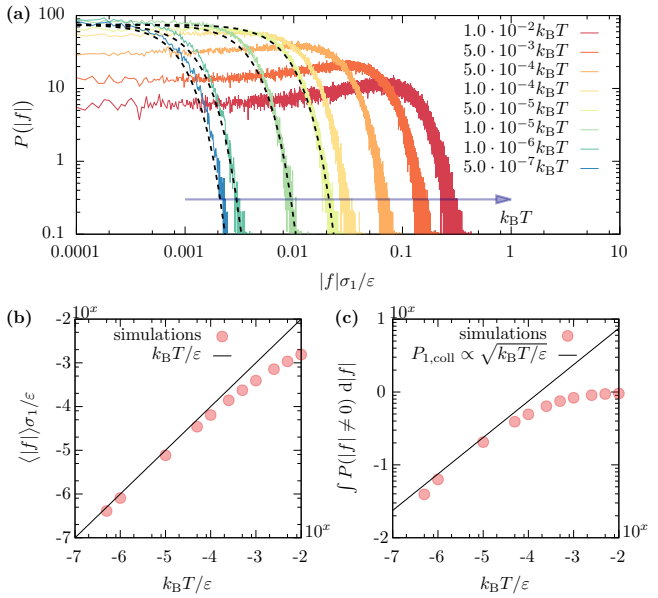

Figure 5. (a) Force distributions $P(|f|)$ depending on the absolute value of interaction forces $|f|$ at a packing fraction of $\phi = 0.54$ for different temperatures T. The colored lines are results of simulations and the black dashed lines are fits according to Eq. (9). The factor according to Eq. (9) has a constant value of $A = 75$. (b) Average of the absolute value of the force as a function of temperature, determined from simulations. The black line is proportional to $k_B T/\varepsilon$. (c) Fraction of non-zero forces, i.e., the normalization of the distributions from (a), where the integral runs only over all non-zero forces. Points are from simulations and the line is proportional to $\sqrt{k_B T/\varepsilon}$.

IV.3. Memory effects

On the way to deduce atomistic descriptions of potential barriers that a particle needs to overcome in order to leave its cage into a given direction, we found out that for a small particle the escape from the cage along the z-axis is a probable process. As it will turn out, it is not sufficient to simply consider a mean potential force as an external field in order to describe the confinement by a local cage. The reason is that within such a simple mean field description there is no memory, i.e., no dependence on the history. Thus, we analyze the importance of memory effects in the following.

In order to access the dependence on the history of a particle, we separately determine the forces for the following two groups of particles: First, particles that at a previous time $-t$ were at a position $z(-t) > z(0)$, i.e., further away from the wall than the current position. Second, particles that were at a previous time $-t$ at a position $z(-t) < z(0)$ closer to the wall. Then, the average forces on a particle are

$$f^{>}_{1,\mathrm{z}}(z,t) = \frac{1}{N_1'} \sum_{i=1}^{N_1'} f_{1,\mathrm{z}}\big(z(0)\big)\theta\big(z(-t) - z(0)\big), \qquad (11)$$

$$f^{<}_{1,\mathrm{z}}(z,t) = \frac{1}{N_1'} \sum_{i=1}^{N_1'} f_{1,\mathrm{z}}\big(z(0)\big)\theta\big(z(0) - z(-t)\big), \qquad (12)$$

where Eq. (11) denotes the forces for particles that in the past have been further away from the wall, while Eq. (12) gives the forces for spheres that previously have been closer to the wall. Again, N_1' is the number of the considered particles only.

Furthermore, we introduce the deviations from the average value $\langle f_{1,\mathrm{z}}(z) \rangle$ and call those functions the force memories, i.e.,

$$\Delta f^{X}_{1,\mathrm{z}}(z,t) = f^{X}_{1,\mathrm{z}}(z,t) - \langle f_{1,\mathrm{z}}(z) \rangle, \qquad (13)$$

with the placeholder $X \in \{<, >\}$. In Fig. 6(a) and (b) we plot the history-dependent force memories for bulk systems with different packing fractions in linear and double logarithmic representation, respectively. As the packing fraction is increased, two major characteristics determine the curves. The first is the starting point of the memory curve, i.e., $\Delta f^{>}_{1,\mathrm{z}}(z, t \to 0)$, which sets the magnitude of the force memory. The second is the timescale, on which the memory approximately decays. For the bulk, we pick out two systems, one being at intermediate packing fraction ($\phi = 0.52$) and the other one at a large density ($\phi = 0.58$) and fit the force memories via stretched exponential functions

$$\Delta f^{>}_{1,\mathrm{z}}(z,t) = \Delta f^{>}_{1,\mathrm{z}}(z) \exp\left[-(t/\tau_{\mathrm{mem}})^{\alpha}\right], \qquad (14)$$

where we fixed the exponent $\alpha = 0.4$, in order to obtain reasonably comparable fits. For the two thick gray lines in Fig. 6(b) the characteristic memory times are $\tau_{\mathrm{mem}} = 187.5\tau_{\mathrm{B}}$ (for $\phi = 0.58$) and $\tau_{\mathrm{mem}} = 6.3\tau_{\mathrm{B}}$ (for $\phi = 0.52$).

Whilst the simulation curves seem to follow such a stretched exponential for short to intermediate times, for very old histories the memories behave like a power-law with an exponent $-1/2$. This is expected, since in an overdamped system our definition of the instantaneous force deviations are supposed to behave similar to the velocity-autocorrelation function (see, e.g., Ref. [30, 31]) that in three dimensions is expected to decay with an exponent of $-3/2$ [32]. Since we restrict the diffusion direction to one direction, our curves should be comparable with the velocity-autocorrelation functions in one dimension with a decay exponent of $-1/2$ [31].

The meaning of the force memory can be interpreted in the following way: as a particle leaves its initial location, in the case of dense systems it has to overcome an effective energy barrier that is caused by its cage. During a short-distance movement the particle already deforms its cage in such a way that the probability of finding a neighboring particle in the direction of its movement

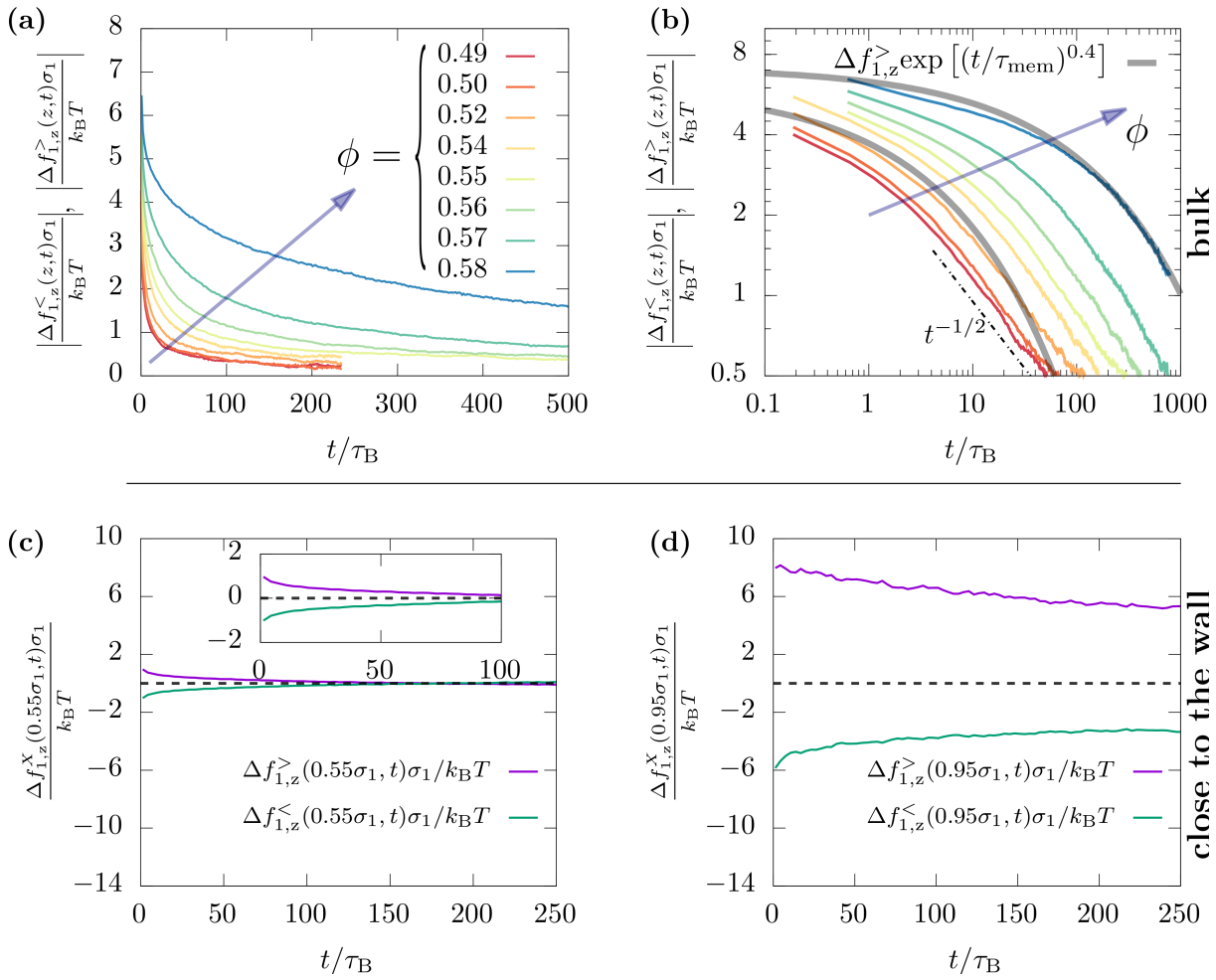

Figure 6. (a,b) Bulk force memories $\Delta f^{<}_{1,z}(z,t)$ and $\Delta f^{>}_{1,z}(z,t)$ defined as deviations of the forces from their average value for particles that have previously been closer to the wall or further away from the wall, respectively. Different packing fractions are considered. Since the bulk limit is considered, z does not matter and the absolute value of the different force memories ($<$ or $>$) coincide. In (a) a linear and in (b) a double-logarithmic representation is shown, respectively. The black dashed line (b) is a power-law with exponent $-1/2$ and the thick gray lines are fits according to $\Delta f^{>}_{1,z}\exp\left[(t/\tau_{\rm mem})^{0.4}\right]$, with $\tau_{\rm mem}\approx 187.5\tau_{\rm B}$ (for $\phi=0.58$) or $\tau_{\rm mem}\approx 6.3\tau_{\rm B}$ (for $\phi=0.52$). (c,d) Force memory close to the wall in the case of the largest considered packing fraction ($\phi=0.58$) for small particles at (c) $z=0.55\sigma_1$ and (d) $z=0.95\sigma_1$. The dashed black lines indicate zero.

increases. At the same time, the probability to lack a neighbor in the opposite direction, i.e., behind the particle, increases. This causes the particle to feel an average force, the force memory, which acts against the direction of its motion. The memory effect is more pronounced for denser systems than for dilute suspension. The timescale of the memory depends on the timescale for relaxation processes in the corresponding systems.

Whereas the force memory does not depend on the position of a bulk particle on average, it does close to the wall. Thus, in Fig. 6(c,d) we show $\Delta f^{X}_{1,z}(z,t)$ for a packing fraction $\phi=0.58$ at wall contact and in between the first two layers. One can nicely see the quantitative difference between the memories at the two investigated positions. For a particle, which is in the first layer and therefore very close to the wall, the force memory has only very subtle impact (Fig. 6(c)). Contrarily, the memory for a particle in between two layers seems to be crucial (Fig. 6(d)).

In Fig. 7(a) the history-dependent forces at short times, i.e. $f^{X}_{1,z}(z,t\to 0)$, and for comparison the average force as functions of the position z are shown. In Fig. 7(b) the respective force memories $\Delta f^{X}_{1,z}(z,t\to 0)$ are plotted. Here, the $t\to 0$ limit was determined by considering the corresponding functions at a time $t=\tau_{\rm B}/3$ which is much shorter than the rearrangement time in all systems.

Intriguingly, as marked by the vertical lines in Fig. 7(b) a connection between maxima of the local density (red line) and the magnitude of the force history (green and blue lines) becomes visible. Whenever a local density peak emerges, the magnitude of the memory is suppressed. The opposite is true for local density minima, where the magnitude of the corresponding force memo-

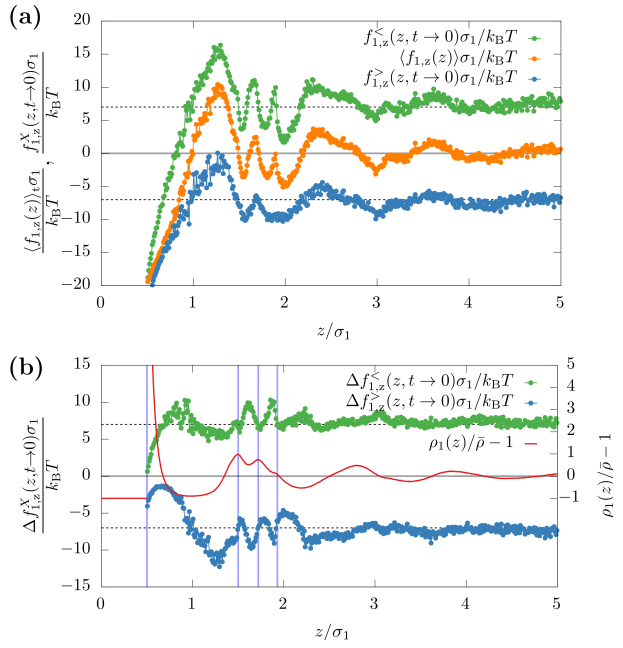

Figure 7. (a) History-dependent forces for small particles at a packing fraction $\phi = 0.58$ as a function of the distance z above the wall for particles that previously have been closer (green line) or further away from the wall (blue line). The previous position was evaluated at a time $-t = -1/3\tau_B$ which approximately corresponds to the limit $t \to 0$. The central orange line corresponds to the average force profile $\langle f_{1,z}(z)\rangle$. (b) Force memories, i.e., deviations from the average force, of the same data as in (a). In addition, the local density profile $\rho_1(z)$ of the smaller particle species (red line, right axis) is shown. The vertical shallow blue lines mark local density maxima (or enhancements) in $\rho_1(z)$ and correspond to local drops of the absolute values of $\Delta f^X_{1,z}(z)$.

ries is enhanced. This shows that when particles reside inside a local density layer, they are supposed to be more stable at this position for longer times and individually occurring forces are similar. In return, this precipitates in the average of the force memory and therefore results in a less pronounced deviation from the total average. On the other hand, when a particle is on its way from one density maximum to another, it necessarily crosses a local minimum. On this crossing, its history has major influence on the average forces. For example, when the particle is moving in positive z-direction, it possibly leaves void space behind it, whereas in front of it a barrier of neighboring particles is blocking its path. Therefore, it is very likely that at such a position the memory has a large effect on the consecutive motion.

V. ONE-PARTICLE RANDOM-WALK MODELS

In this section, we test whether a random-walk model for a single particle can describe a cage breaking event. We will not construct a model that is just based on an escape rate like Kramer's rate (see, e.g., [33]) or on an escape rate given in an free energy landscape as detmined in [34] but our random walks rely on the ingredients obtained in the previous section. To analyze the impact of the different ingredients, we construct random walk models where one particle in principle moves in three dimensions, though we use the models to describe the cage-breaking motion along the z-axis. We employ the diffusion coefficients as given by the temperature in order to determine the mean square of a step length and the average force profile in order to obtain a drift contribution in the case the particle is overlapping with another particle. The probability for a collision as determined from simulation data is used as an additional input in order to decide whether there is any overlap at all. In the first model, no history-dependence is used, while in the second model we employ the memory function obtained from our simulations as an additional input. We will employ the test case, where a single small particle starts at the wall and moves towards the second layer in a perpendicular straight path.

V.1. Random-walk model without memory

Our first random-walk model (RW, no mem.) does not incorporate any memory. It just employs the average force $\langle f_{1,z}(z)\rangle$ acting on a particle. The model consists of the following steps:

1. Decide from an equally distributed random number and from the z-dependent collision probability $P_{1,\mathrm{coll}}(z)$, whether the particle collides with another particle.

2. Calculate a three-dimensional diffusion step $\Delta\vec{r}^{\,\mathrm{step}}$ within a time Δt^{step} via a diffusion coefficient according to free diffusion and an external force in the case of a collision.

According to these steps, the external force vanishes if no collision occurs, but in the case of a collision an external force $\vec{f}^{\,\mathrm{step}} = \vec{f}^{\,\mathrm{step},1} + \vec{f}^{\,\mathrm{step},2}$ with the following two contributions is applied:

$$\vec{f}^{\,\mathrm{step},1} = -\frac{\Delta\vec{r}^{\,\mathrm{step}}}{|\Delta\vec{r}^{\,\mathrm{step}}|}\frac{\langle|\vec{f}_{1,\perp}(z)|\rangle}{P_{1,\mathrm{coll}}(z)}, \tag{15}$$

$$\vec{f}^{\,\mathrm{step},2} = \vec{e}_z\frac{\langle f_{1,z}(z)\rangle}{P_{1,\mathrm{coll}}(z)}. \tag{16}$$

Here, $\langle|\vec{f}_{1,\perp}(z)|\rangle$ is the average of the absolute (normal) forces acting on the particles surface at a position z. It is proportional to the local average pressure and can be calculated from the one-particle density together with the anisotropic pair correlations. The second force is the mean force, exerted by the structure of the neighboring particles. In both cases the normalization with the collision probability $P_{1,\mathrm{coll}}(z)$ guarantees that the average force profile $\langle f_{1,z}(z)\rangle$ is recovered over time.

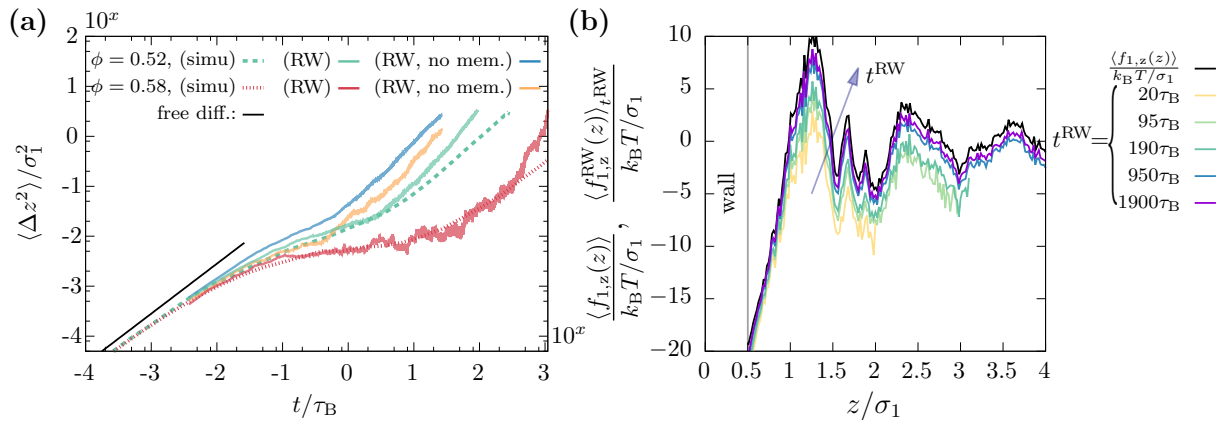

Figure 8. (a) MSDs in z-direction for small particles starting at the wall. The plot shows data for two different packing fractions $\phi = 0.52$ and $\phi = 0.58$ in comparison to the data for a free particle (black solid line). The dashed lines are obtained from our multi-particle simulations, whereas the colored shallow lines are calculated from our random-walk models with (RW) and without (RW, no mem.) history-dependent memory. (b) Measured (average) position-dependent force in the random-walk model RW with incorporation of memory after different runtimes. In the limit of infinite runtime, the random-walk model RW predicts the same average force as our multi-particle simulation (black solid line).

V.2. Random-walk model with memory

Our second random-walk model (RW) incorporates the memory of the history of the particle, namely the fact that it has started at the wall and, for this reason, is supposed to recognize the impact of the force memory $\Delta f_{1,z}^{<}(z,t)$. In this model the second force $\vec{f}^{\,\mathrm{step},2}$ of the model RW, no mem. is slightly modified such that it reads

$$\vec{f}^{\,\mathrm{step},2} = \vec{e}_z \frac{\langle f_{1,z}(z)\rangle + \Delta f_{1,z}^{<}(z)\exp\left[-(t/\tau_{\mathrm{mem}})^{0.4}\right]}{P_{1,\mathrm{coll}}(z)}, \tag{17}$$

where we use the fits of the force memories from Eq. (14) as an input and the respective parameters as indicated in Fig. 6(b).

V.3. Comparison of the random-walk predictions and simulation results

In Fig. 8(a) we plot the MSD of small particles in z-direction for simulation data in comparison with results from our random-walk models for two different packing fractions. In case of the history-dependent model RW the respective memory times are $t_{\mathrm{mem}} = 187.5\tau_B$ for $\phi = 0.58$ and $t_{\mathrm{mem}} = 6.3\tau_B$ for $\phi = 0.52$. For the simple random-walk model RW, no mem. without memory, the curves deviate from the measured ones already at small runtime t. The deviation is less pronounced for the dilute system, where memory is supposed to play a smaller role than for systems close to the glass transition. The model RW (with memory) leads to reasonable predictions with, at least, a typical rearrangement for both packing fractions. The impact of memory in our model system is illustrated in Fig. 8(b), where we plot the average measured forces as a function of the particle position z and of the runtime τ_{RW}. For short runtime, the particle does not manage to hop over the first few particle layers, which results in truncated lines. However, for increasing runtime, the time-averaged forces from our random walk models converge, as expected, against $\langle f_{1,z}(z)\rangle$. This mimics the loss of memory.

VI. CONCLUSIONS

In this work we explored the properties of a cage-breaking event in a bidisperse mixture of spheres in the vicinity of a wall. We studied the ingredients which are necessary to develop an effective one-particle random-walk description of the dynamics. By considering cages close to a wall and an escape route perpendicular to the wall, we guaranteed that errors that arise due to averaging quantities over differently oriented cages are small. We discovered that a random-walk model can describe the dynamics reasonably well if a suitable anisotropic force distribution, a collision frequency, and a memory function are used as input. While the force distribution and the collision frequency in principle can be obtained from theories on a level of two-particle structural correlations (as studied in previous works [13, 15]), the memory of a trajectory depends on the motion of all particles in the surrounding cage. Besides the memory function, no other collective motion effects had to be included. By this, we demonstrated that the memory is essential to describe the dynamics in a dense system.

In order to develop comparable random-walk models for rearrangements in bulk, one has to be careful with averages over different cage orientations. In principle, it should be possible to construct such random-walk models following three steps. First, all relevant (probable)

cages in bulk must be identified (cf. [35]). Second, the distributions of forces must be determined for all these cage configurations in such a way that the orientation is always fixed relative to one neighboring particle. Third, the average over orientations must be calculated. That way, the dynamics along the escape route and along other directions can be determined independently before taking an average instead of determining the dynamics after averaging over directions, which would correspond to the dynamics based on an isotropic mean field cage. Thus, errors can be avoided which result from the fact that the averaging over directions and the determination of escape dynamics obviously do not commute. It would be interesting to investigate how our approach compares to free energy landscapes of a cage [34] or how our results can be built in or compared to the theories which employ isotropic cages, e.g., the theory where the cage breaking event is facilitated by the elasticity of the cage [12] or mode coupling theory [5, 14].

ACKNOWLEDGEMENTS

M.K. and M.S. are supported within the Emmy Noether program of the Deutsche Forschungsgemeinschaft (Grant Schm 2657/2). A.H. acknowledges financial support from the DFG within the priority program SPP 1726 (grant number SP 1382/3-1).

[1] Hoover W G and Ree F H 1968 *J. Chem. Phys.* **49** 3609–3617
[2] Woodcock L V 1976 *J. Chem. Soc., Faraday Trans. 2* **72**(0) 1667–1672
[3] Pusey P N and van Megen W 1986 *Nature* **320** 340–342
[4] Kirkpatrick T R 1985 *Phys. Rev. A* **31**(2) 939–944
[5] Götze W and Sjögren L 1992 *Rep. Prog. Phys.* **55** 241–376
[6] Santen L and Krauth W 2000 *Nature* **405** 550–551
[7] Schweizer K S and Saltzman E J 2004 *J. Phys. Chem. B* **108** 19729–19741
[8] Schweizer K S 2005 *J. Chem. Phys.* **123** 244501
[9] Elmatad Y S, Chandler D and Garrahan J P 2009 *J. Phys. Chem. B* **113** 5563–5567
[10] Granato A V 2011 *J. Non-Cryst. Solids* **357** 334–338
[11] Mirigian S and Schweizer K S 2013 *J. Phys. Chem. Lett.* **4** 3648–3653
[12] Dell Z E, Tsang B, Jiang L, Granick S and Schweizer K S 2015 *Phys. Rev. E* **92**(5) 052304
[13] Härtel A, Kohl M and Schmiedeberg M 2015 *Phys. Rev. E* **92**(4) 042310
[14] Götze W 2008 *Complex Dynamics of Glass-Forming Liquids: A Mode-Coupling Theory* International Series of Monographs on Physics (OUP Oxford)
[15] Götzelmann B, Haase A and Dietrich S 1996 *Phys. Rev. E* **53**(4) 3456–3467
[16] Evans R, Oettel M, Roth R and Kahl G 2016 *J. Phys Condens. Matter* **28** 240401
[17] Hansen-Goos H and Roth R 2006 *J. Phys. Condens. Matter* **18** 8413–8425
[18] Härtel A, Oettel M, Rozas R E, Egelhaaf S U, Horbach J and Löwen H 2012 *Phys. Rev. Lett.* **108**(22) 226101
[19] Oettel M, Dorosz S, Berghoff M, Nestler B and Schilling T 2012 *Phys. Rev. E* **86**(2) 021404
[20] Malijevský A, Yuste S B, Santos A and López de Haro M 2007 *Phys. Rev. E* **75**(6) 061201
[21] Davidchack R L, Laird B B and Roth R 2016 *Condens. Matter Phys.* **19** 23001
[22] Rowlinson J 1964 *Mol. Phys.* **7**(4) 349–361
[23] Barker J A and Henderson D 1967 *J. Chem. Phys.* **47** 4714–4721
[24] Andersen H C, Weeks J D and Chandler D 1971 *Phys. Rev. A* **4**(4) 1597–1607
[25] Xu N, Haxton T K, Liu A J and Nagel S R 2009 *Phys. Rev. Lett.* **103**(24) 245701
[26] Schmiedeberg M, Haxton T K, Nagel S R and Liu A J 2011 *EPL* **96** 36010
[27] Haxton T K, Schmiedeberg M and Liu A J 2011 *Phys. Rev. E* **83**(3) 031503
[28] López-Flores L, Ruíz-Estrada H, Chávez-Páez M and Medina-Noyola M 2013 *Phys. Rev. E* **88**(4) 042301
[29] Hansen J P and McDonald I R 2013 *Theory of simple liquids* 4th ed (Elsevier)
[30] Alder B J and Wainwright T E 1970 *Phys. Rev. A* **1**(1) 18–21
[31] Pomeau Y and Résibois P 1975 *Phys. Rep.* **19** 63–139
[32] Ernst M, Machta J, Dorfman J and van Beijeren H 1984 *J. Stat. Phys.* **34** 477–495
[33] Hänggi P, Talkner P and Borkovec M 1990 *Rev. Mod. Phys.* **62**(2) 251–341
[34] Ekimoto T, Yoshimori A, Odagaki T and Yoshidome T 2013 *Chem. Phys. Lett.* **577** 58–61
[35] Royall C P, Malins A, Dunleavy A J and Pinney R 2015 *J. Non-Cryst. Solids* **407** 34–43